Content

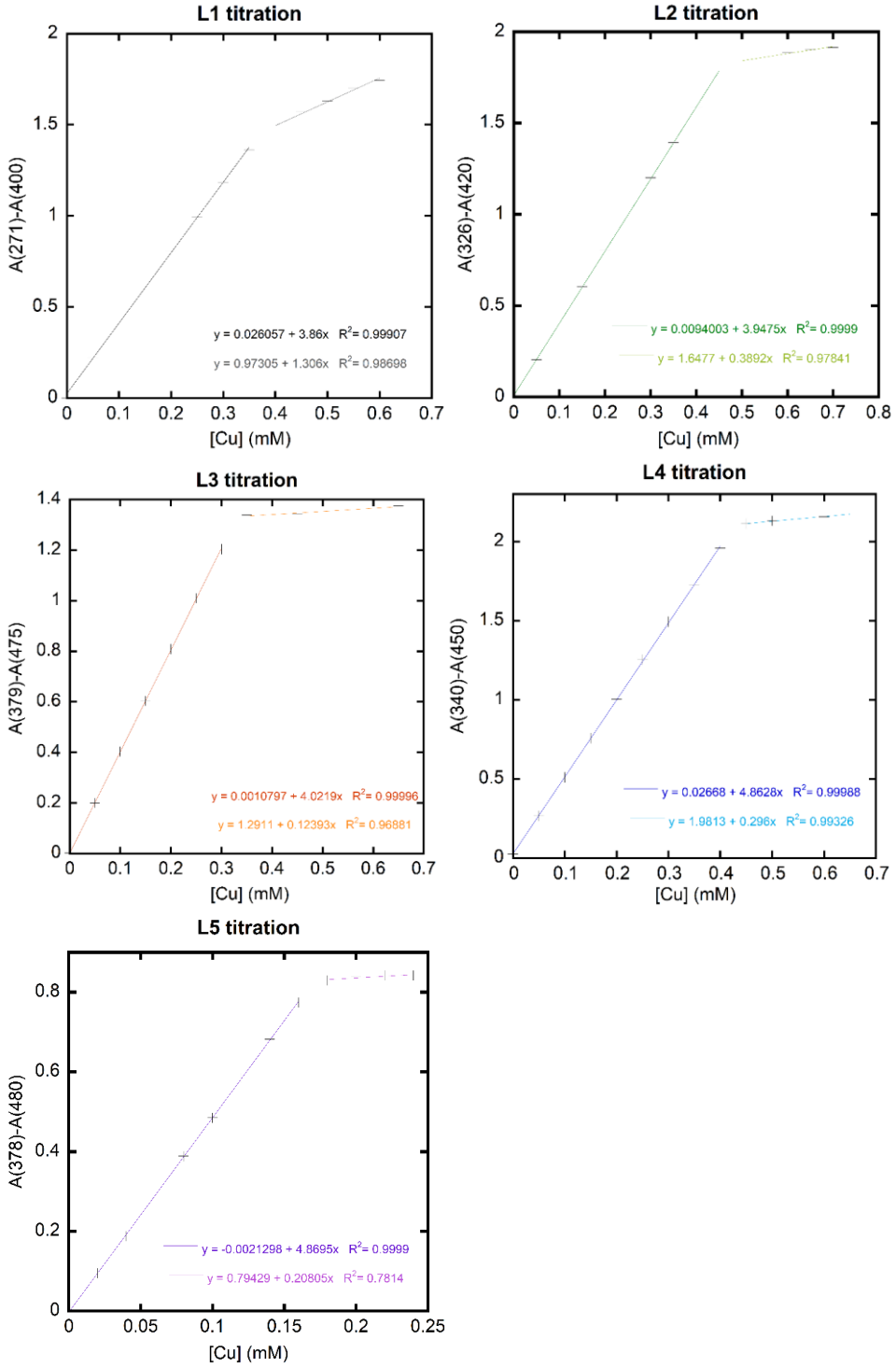

Figure S1. Illustration of titrations of **L1** to **L5** by addition of [Cu(II)], followed by UV-vis spectroscopy. Titrations are repeated at least three times. [**Li**] ≈ 500 µM for i=1-4, [**L5**] ≈ 200 µM, [Cu(II)] increases by steps of 50 µM, [HEPES] = 100 mM, pH 7.4. The LMCT band near 400 nm is monitored.

Concentrations of stock solutions of ligands based on weight was: 20 mM for **L1**-**L4** and 4 mM for **L5**. The real concentration (average of several titration experiments) give the following real concentration: [**L1**] = 12 mM ; [**L2**] = 18 mM; [**L3**] = 13.3 ; [**L4**] = 17.2 mM and [**L5**] = 3.5 mM respectively. This indicates two main points: the complex formed are 1:1 and the ligands are hydrated.

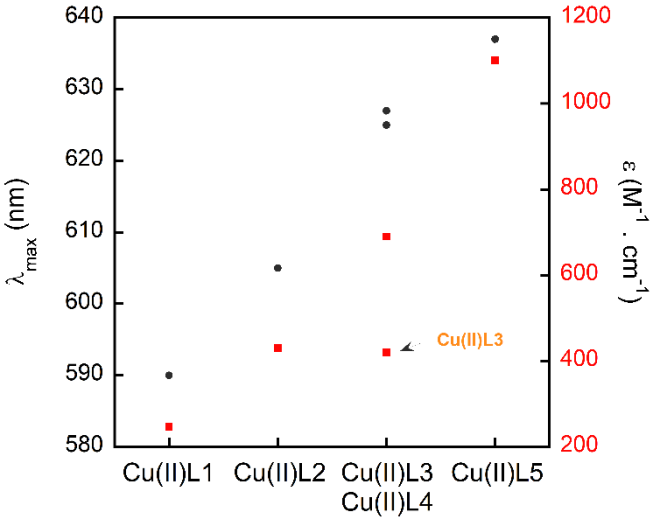

Figure S2. Correlation between the sulfur atom number in the Cu(II)**Li** complexes and both λ_{max} (nm) and ε ($M^{-1}.cm^{-1}$) using data in Table 1.

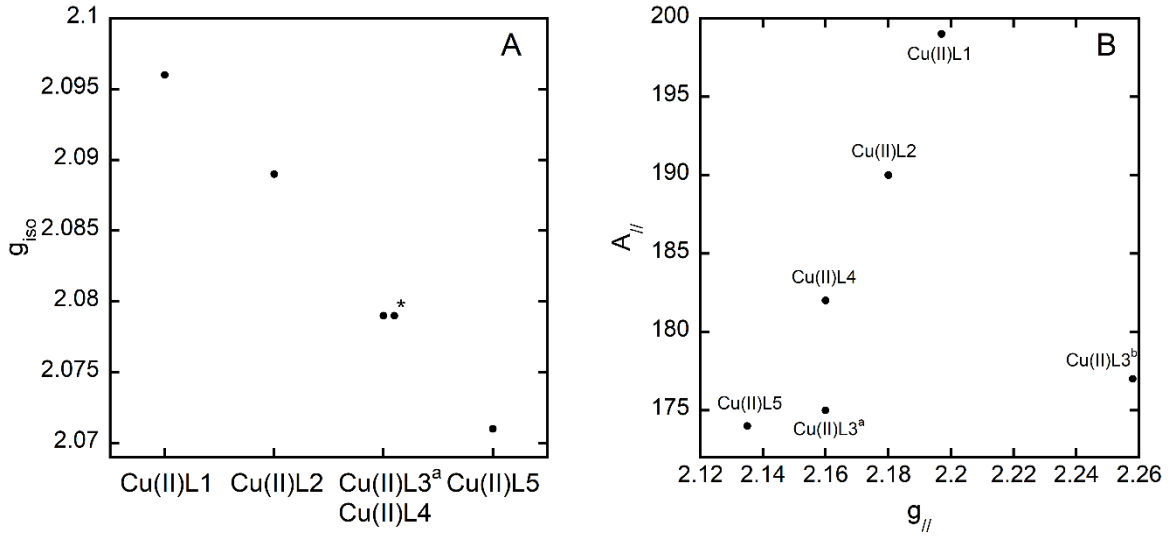

Figure S3. (A) Correlation between the sulfur atom number in Cu(II)**Li** and g_{iso} using simulated data reported in Table 1. For Cu(II)**L3**, only the values related to Cu(II)**L3**^{a} are reported. * artificially shifted to be observed. NB: the value corresponding to Cu(II)**L3**^{b} is g_{iso} = 2.12 and has not been plotted for clarity. (B) Correlation between $A_{//}$ and $g_{//}$ using simulated data reported in Table 1.

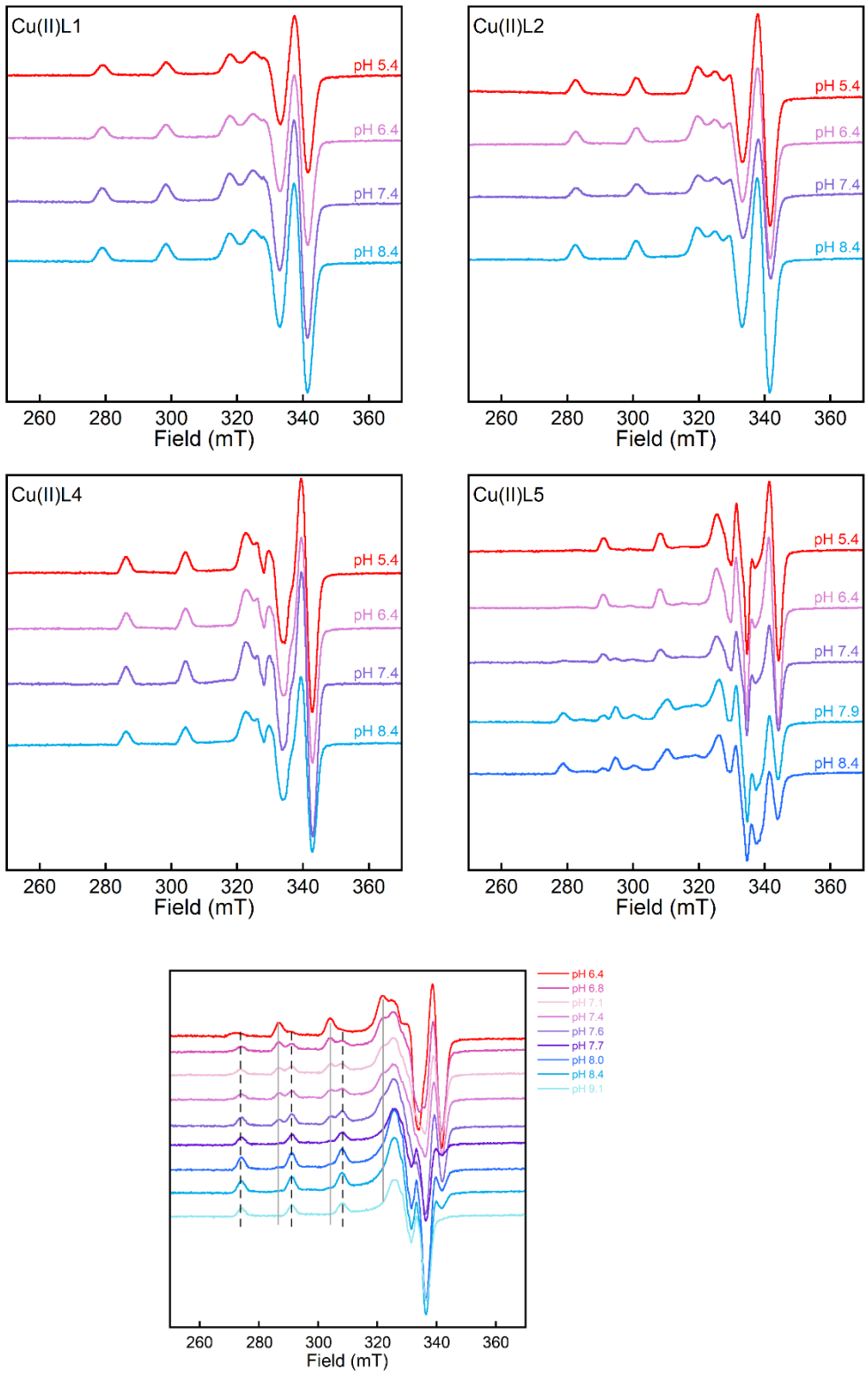

Figure S4. X-band EPR spectra of Cu(II)**L1,** Cu(II)**L2**, Cu(II)**L4** and Cu(II)**L5** at different pH from 6.4 (red) to 8.4 (blue) and of Cu(II)**L3** at different pH from 6.4 (red) to 9.1 (light blue). Experimental conditions [**Li**] = 600 µM, [^{65}Cu(II)] = 500 µM, [HEPES] = 100 mM 10 % of glycerol as cryoprotectant, 120 K.

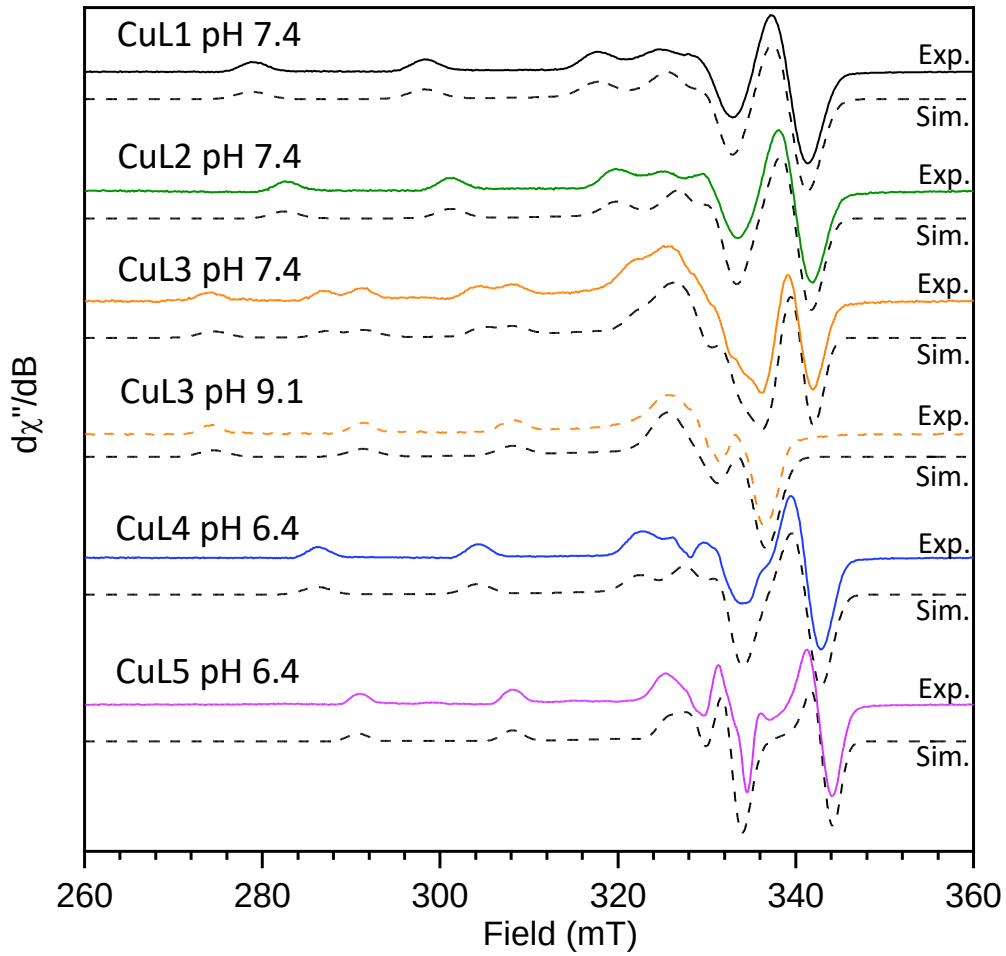

Figure S5. Simulations of the EPR spectra corresponding to Cu(II)**Li** (I = 1 -5) that predominate at physiological pH (Spectra with one main species has been chosen for the matter of simplicity). In case of Cu(II)**L3**, the pH 7.4 spectra has been calculated as the weighted sum of Cu(II)**L3**^{a} and Cu(II)**L3**^{b} (40/60)**,** with parameters fixed for Cu(II)**L3**^{b} (obtained from simulation of the spectrum at pH 9.1).

EPR spectra were simulated by using the Easyspin software package[1] and routines written in the lab. The Cu(II) centers were defined by their g-values and hyperfine couplings. Superhyperfine couplings with relevant nitrogen nuclei was also included. Anticorrelated g- and A- strains were used on Cu(II) to better simulate linebroadening observed experimentally.

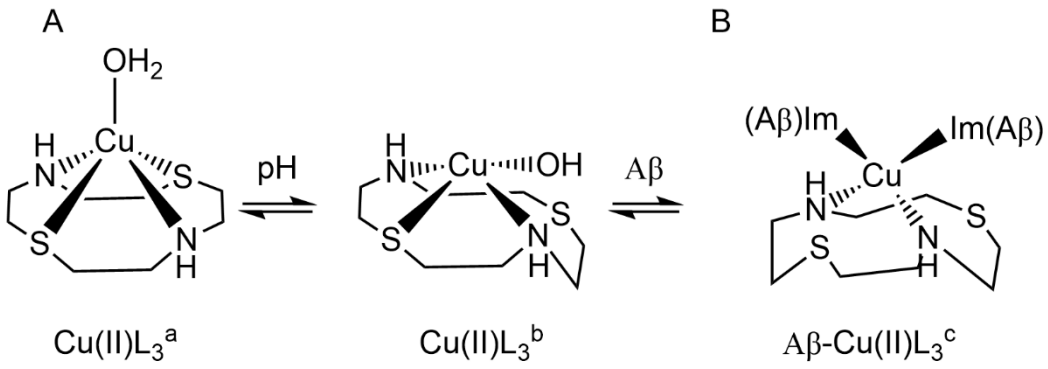

Scheme S1. Proposed Cu(II) coordination sites for **L3** (A) and for Aβ-Cu(II)**L3**^{c} (B).

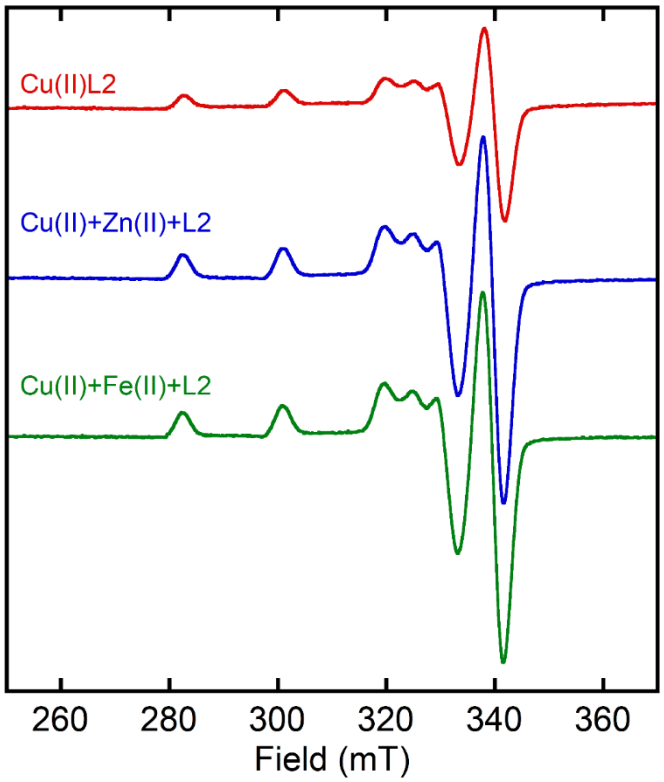

Figure S6. X-band EPR spectra of Cu(II)**L2** (red) in the presence of Zn(II) (blue) or Fe(II) (green). [L2] = 600 µM, [^{65}Cu(II)] = [Zn(II)] = [Fe(II)] = 500 µM, [HEPES] = 100 mM, pH 7.4, 10% of glycerol as cryoprotectant, 120 K.

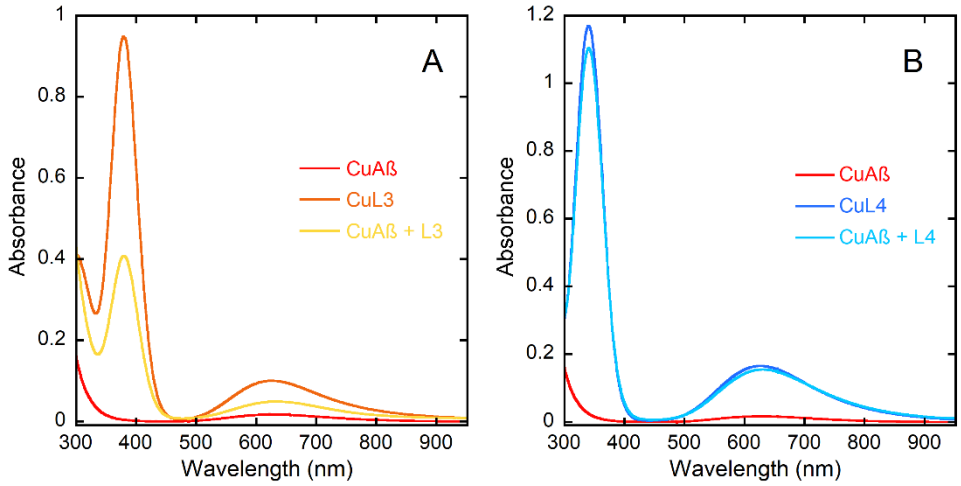

Figure S7. UV-Vis signature of Cu(II)Aβ_{16} and **L3 (A)** or **L4 (B)**. **(A)** Cu(II)Aβ_{16} (red curve), Cu(II)**L3** (orange curve), Cu(II) + Aβ_{16} + **L3** (yellow curve), **(B)** Cu(II)Aβ_{16} (red curve), Cu(II)**L4** (dark blue curve), Cu(II) + Aβ_{16} + **L4** (light blue curve). Condition : [Cu(II)] = 240 µM, [**Li**, Aβ_{16}] = 290 µM, [HEPES] = 100 mM, pH 7.4, T = 25 °C.

Table S1

Ligand	pK_D apparent at pH 7.4 for Cu(II)	Refs.
L1	17.9	2
	19.2	3
L2	15.0 ; 14.7 [a, this work]	3
L3	9.9	4
L4	12.2	4
L5	7.9 [b]	5
no3pa (tris-picolylamine-1,4,7-triazacyclononane)	12.9 ; >16 [c, this work]	6
HSA (human serum albumin)	12.0	7,8
$A\beta_{16}$	9-10	9
L'	14.5	9

[a]: Determined by direct UV-Vis competition with the N,N'-Bis[(5-sulfonato-2-hydroxy)benzyl]-N,N'-dimethyl-ethane-1,2-diamine) = **L'** ligand,[10] after reaching the thermodynamic equilibrium (about one week). [b], corresponds to the Cu(II) + **L5** reaction, the protonation of the ligand being not reported. [c] Determined by direct UV-Vis competition with **L'**,[10] after reaching the thermodynamic equilibrium.

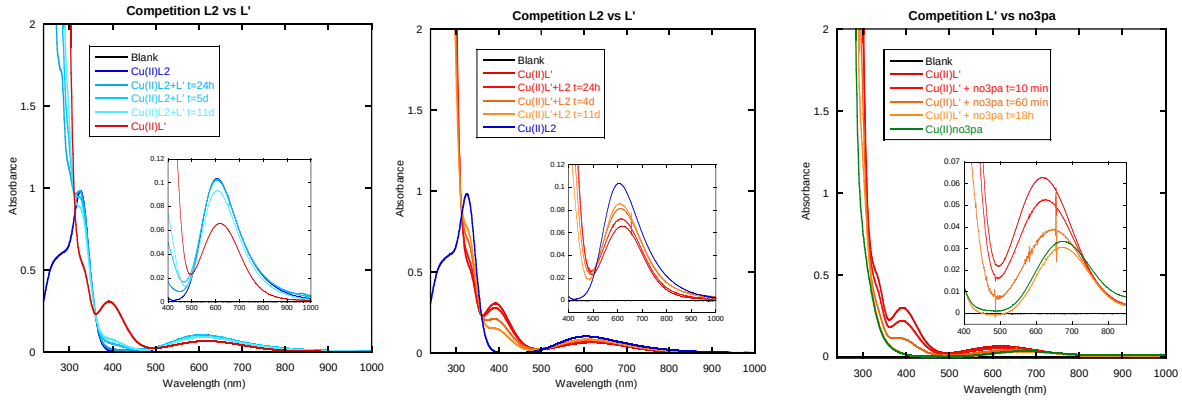

<u>Figure-Table S1.</u> UV-Vis spectra of ligand exchange of Cu(II)(ligand) with addition of another ligand, ligand = **L2**, no3pa or **L'**. Condition : [Cu(II)] = 240 µM, [ligand] = 290 µM, [HEPES] = 100 mM, pH 7.4, T= 25°C.

Based on the extrapolation of the values obtained after 11 days of incubation of the mixtures Cu(II)**L2** + **L'** or Cu(II)**L'** + **L2**, the relative proportion of Cu(II)**L2**:Cu(II)**L'** is estimated at 60:40. Hence the affinity value of Cu(II) for **L2** is deduced from that of **L'** ($3 \times 10^{14} M^{-1}$)[9] to be $4.5 \times 10^{14} M^{-1}$.

After 1 day of incubation of the mixture Cu(II)**L'** + no3pa leads to the complete removal of Cu(II) from Cu(II)**L'**, indicating that no3pa has a much higher affinity than **L'** (at least one order of magnitude higher).

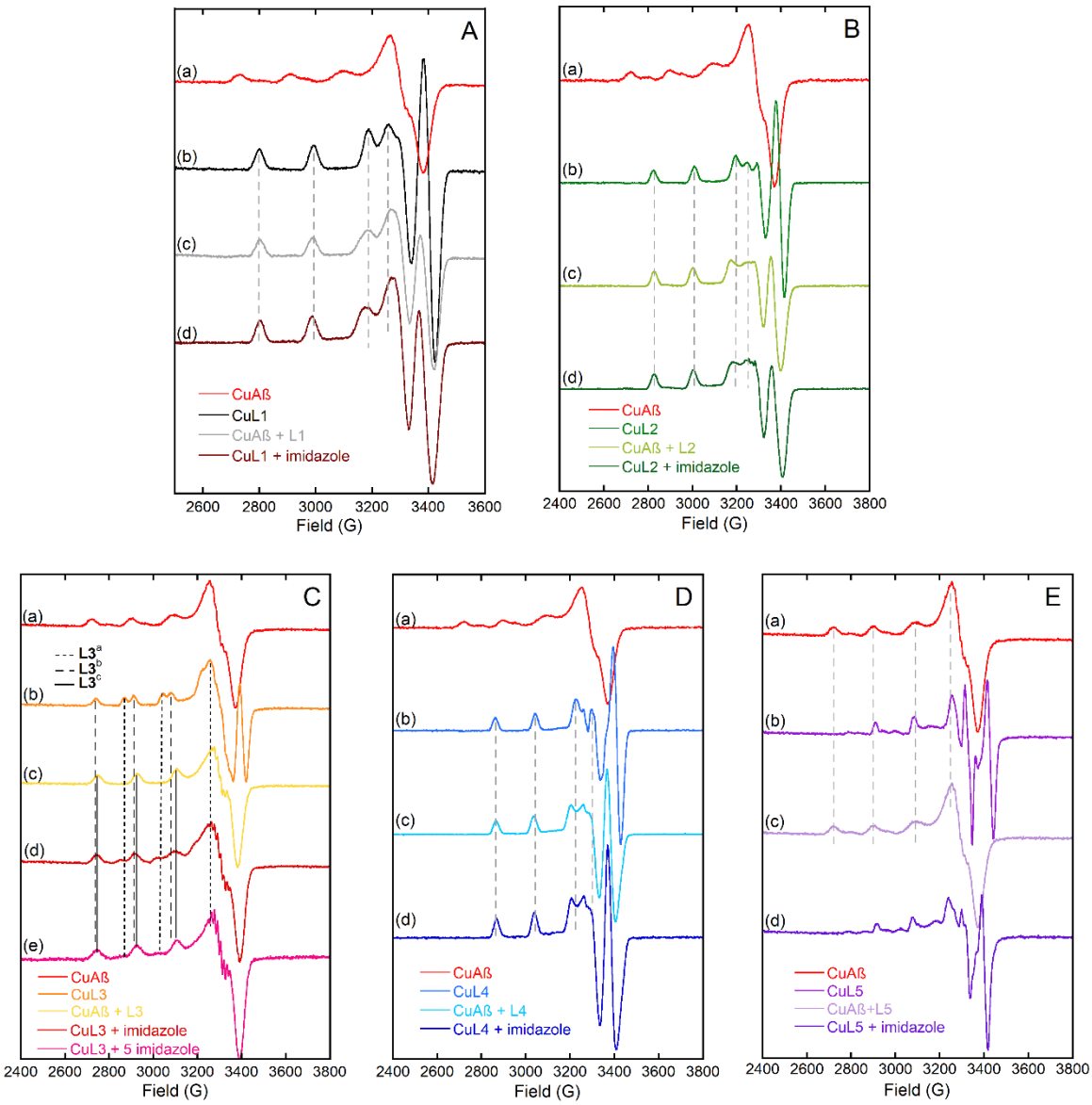

Figure S8. X-band EPR spectra of (a) Cu(II)Aβ_{16}, (b) Cu(II)**Li**, (c) Cu(II)Aβ_{16} + **Li**, (d) Cu(II)**Li** + imidazole (Im) and (e) Cu(II)**Li** + 5 eq. imidazole (Im) for **L1** panel **(A), L2** panel **(B), L3** panel **(C), L4** panel **(D)** and **L5** panel **(E).** Experimental conditions [**Li**, Aβ_{16}, Im] = 600 µM, [^{65}Cu(II)] = 500 µM, [HEPES] = 100 mM, pH 7.4, 10 % of glycerol as cryoprotectant, 120 K. For the panel C, the three different species (**L3**^{a}, **L3**^{b} and **L3**^{c}) have been marked with different line styles. Note that panel A is not at the same scale due to data recording settings.

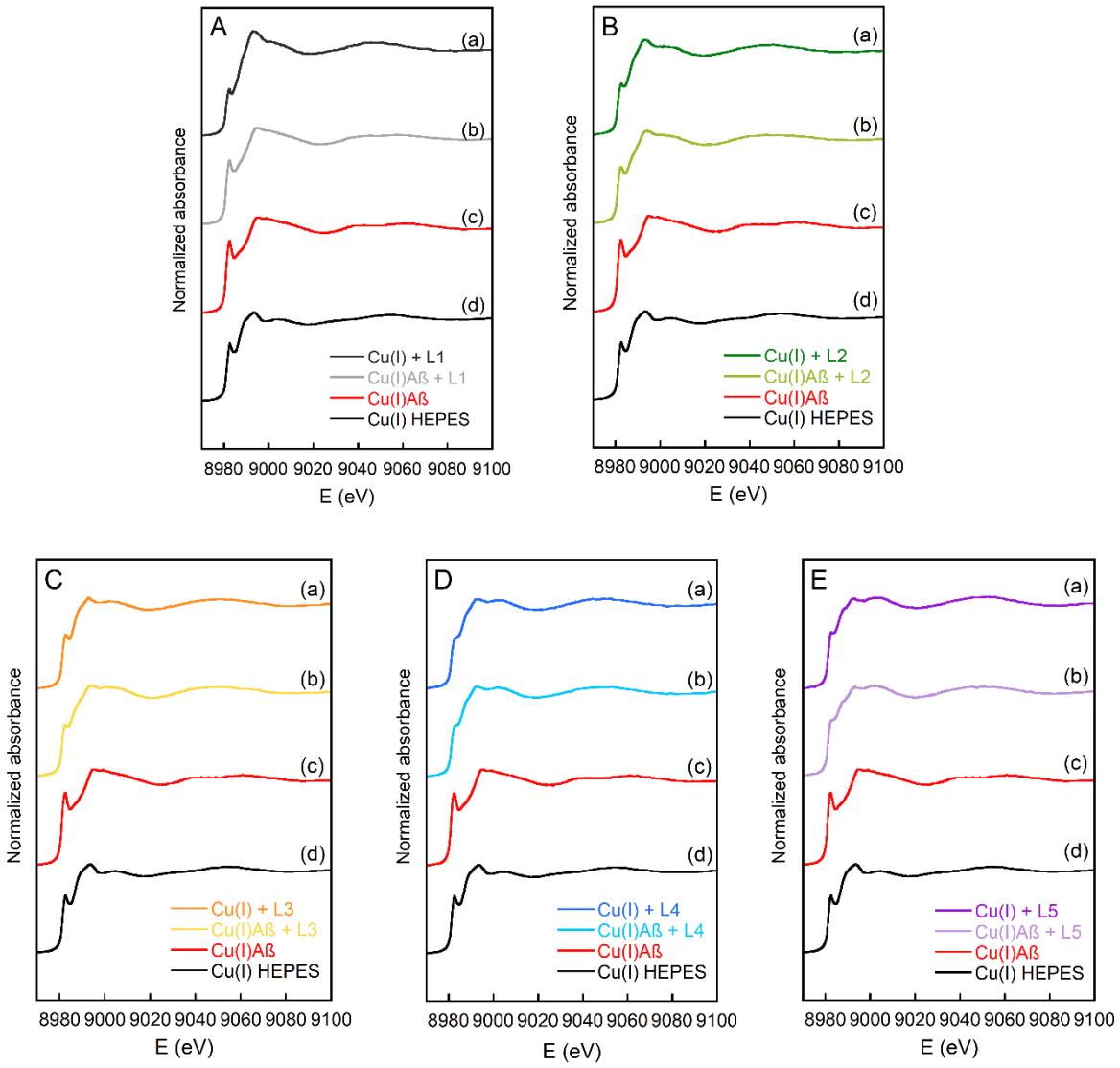

Figure S9. X-ray absorption near edge structure (XANES) spectra of (a) Cu(I)**Li**, (b) Cu(I)Aβ_{16} + **Li**, (c) Cu(I)Aβ_{16} and (d) Cu(I) in HEPES for **L1** panel **(A)**, **L2** panel **(B)**, **L3** panel **(C)**, **L4** panel **(D)** and **L5** panel **(E)**. Conditions: [Cu(II)]= 0.9 mM, [**Li**] = [Aβ_{16}] = 1 mM, [HEPES] = 50 mM, pH 7.4. Copper was reduced with dithionite at 10 mM and the solution was kept under an Ar atmosphere. Glycerol 10% v/v was used as a cryoprotectant. T = 20 K.

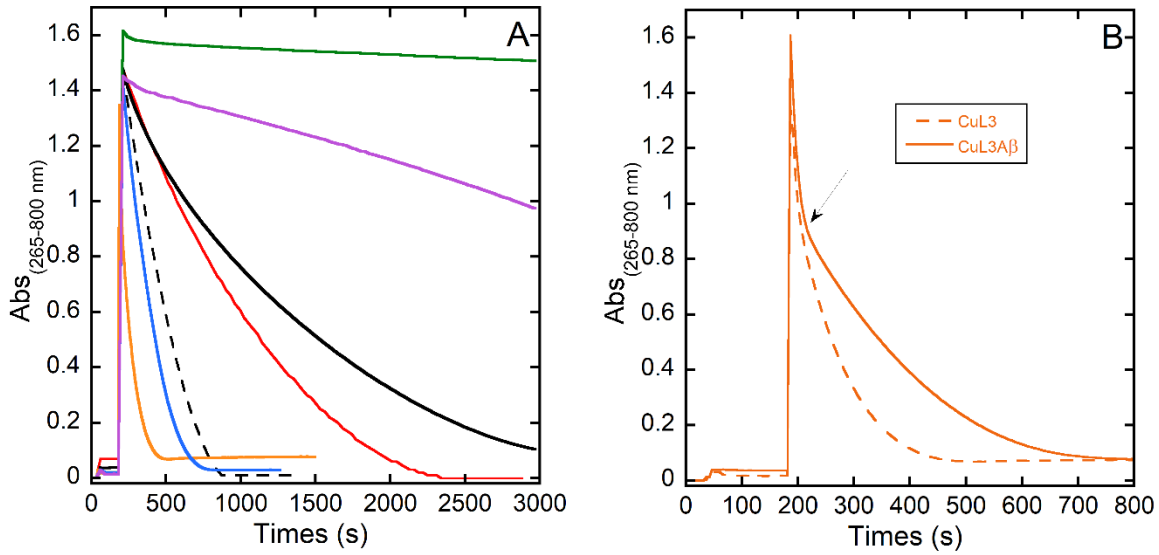

Figure S10. Kinetics of ascorbate consumption, followed by UV-visible spectroscopy at 265 nm starting from Cu(II). Panel **(A)**: Cu(II) + $A\beta_{16}$ (red curve as a control), Cu(II) + Asc (discontinuous black curve), Cu(II) + Asc in the presence of **L1** (black curve), **L2** (green curve), **L3** (orange curve), **L4** (blue curve) and **L5** (violet curve). Panel **(B)** is a zoom at the beginning of the kinetics for **L3** to better view the two slopes of the ascorbate consumption when $A\beta_{16}$ is present, the slope break is indicated by an arrow. Conditions: [**Li**, $A\beta_{16}$] = 12 µM, [Cu(II)] = 10 µM, [Asc] = 100 µM, [HEPES] = 100 mM, pH 7.4 at T = 25 °C.

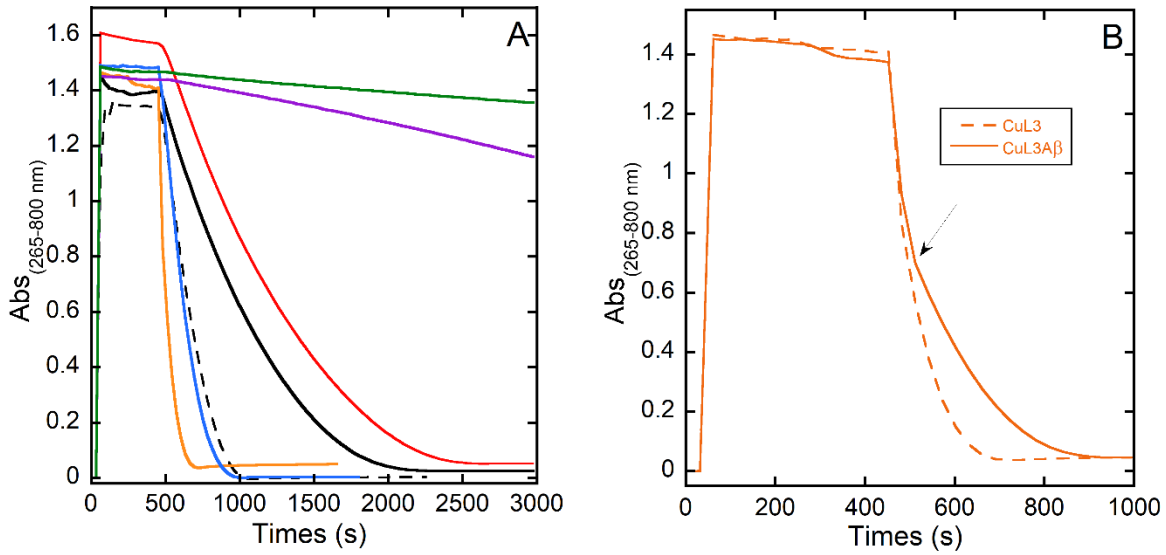

Figure S11. Kinetics of ascorbate consumption, followed by UV-visible spectroscopy at 265 nm starting form Cu(I). Panel **(A)** : Asc + Cu(II) + $A\beta_{16}$ (red curve as a control), Asc + Cu(II) (discontinuous black curve), Asc + Cu(II) in the presence of **L1** (black curve), **L2** (green curve), **L3** (orange curve), **L4** (blue curve) and **L5** (violet curve). Panel **(B)** is a zoom at the beginning of the kinetics for **L3** to better view the two slopes of the ascorbate consumption when Aβ is present, the slope break is indicated by an arrow. Starting from Cu(I), order of additions: Cu(II) + Asc + **Li**. [**Li**, $A\beta_{16}$] = 12 µM, [Cu(II)] = 10 µM, [Asc] = 100 µM, [HEPES] = 100 mM, pH 7.4 at T = 25 °C.

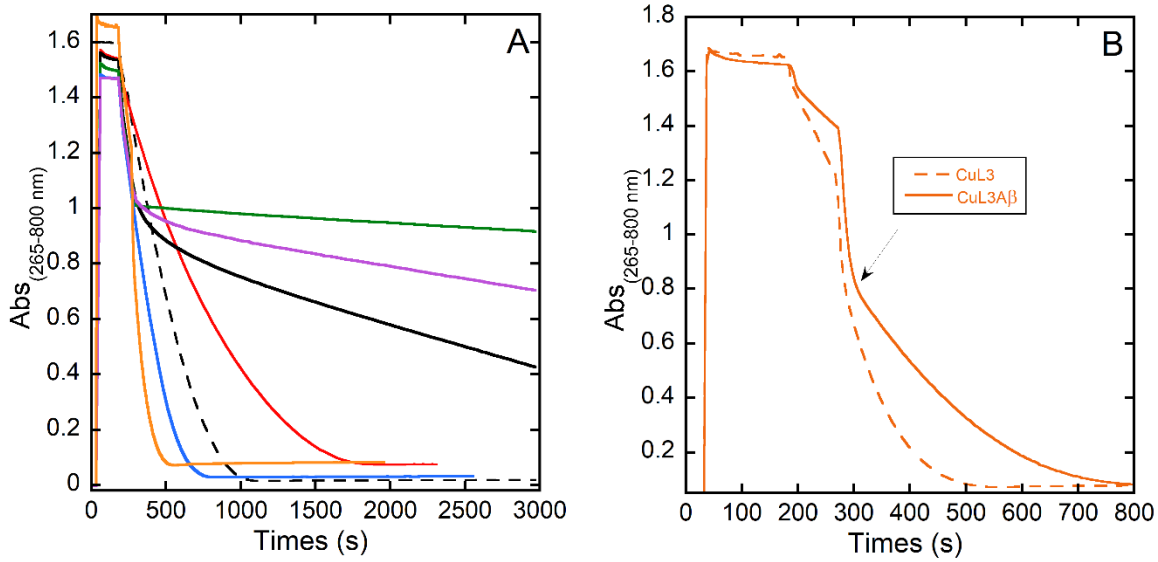

Figure S12. Kinetics of ascorbate consumption, followed by UV-visible spectroscopy at 265 nm starting from Cu(I)/Cu(II). Panel **(A)**: Asc + Cu(II) + $A\beta_{16}$ (red curve as a control), Asc + Cu(II) (discontinuous black curve), Asc + Cu(II) in the presence of **L1** (black curve), **L2** (green curve), **L3** (orange curve), **L4** (blue curve) and **L5** (violet curve). Panel **(B)** is a zoom at the beginning of the kinetics for **L3** to better view the two slopes of the ascorbate consumption when Aβ is present, the slope break is indicated by an arrow. Order of addition: Asc + Cu(II) + **Li**. Conditions [**Li**, $A\beta_{16}$] = 12 µM, [Cu(II)] = 10 µM, [Asc] = 100 µM, [HEPES] = 100 mM, pH 7.4 at T = 25 °C.

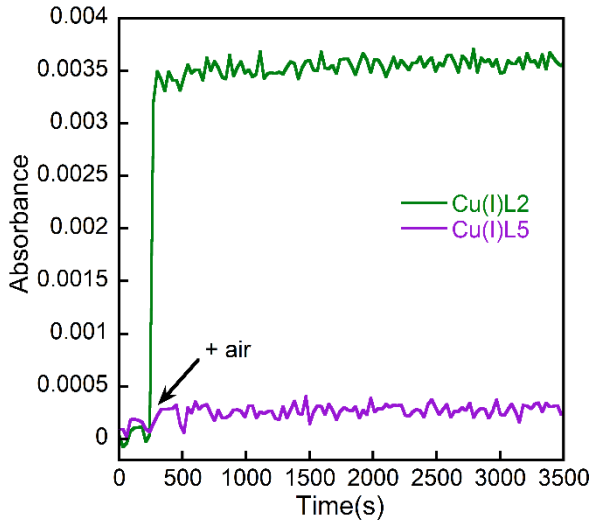

Figure S13. Plot of the maximum absorbance at λ_{max} of the d-d transition of the complexes Cu**L2** (green) and Cu**L5** (violet) as a function of time during the ROS experiment starting from Cu(I). At the beginning of the kinetic A = 0 due to the absence of Cu(II). At 250 s the UV-vis cuvette is opened to air allowing the Cu(I)**Li** to be oxidized. [Cu] = 10 µM, [**Li**] = 12 µM, [Asc] = 100 µM, [HEPES] = 100 mM, pH 7.4, T = 25 °C.

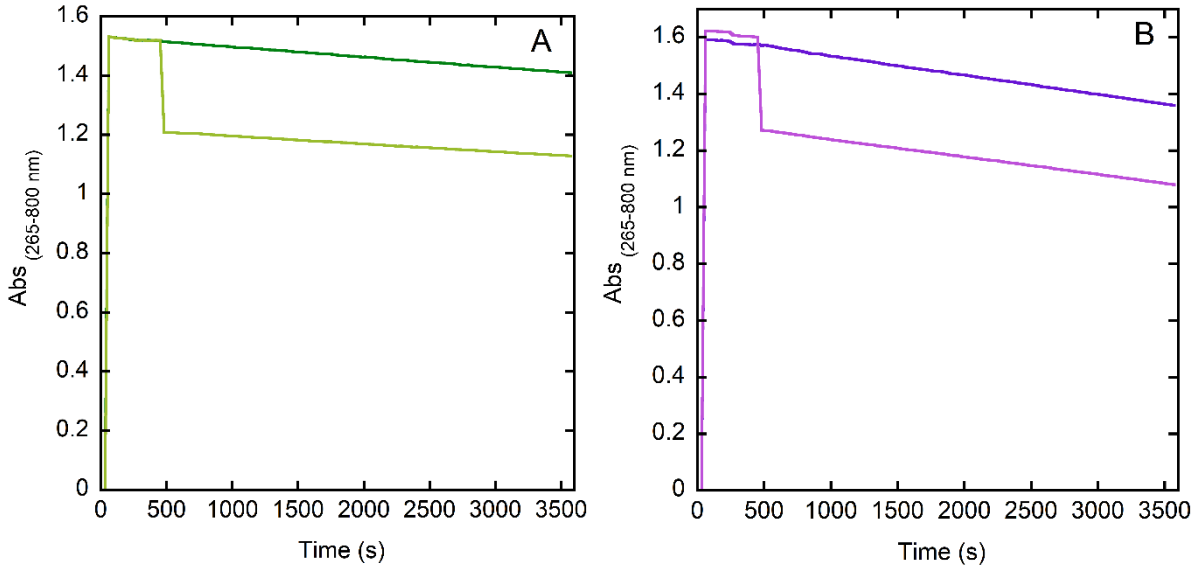

Figure S14. Kinetics of ascorbate consumption followed by UV-visible spectroscopy at 265 nm starting from Cu(I) in the presence of (A) **L2**, (B) **L5**. At 500 s, addition of O_2 was performed by opening the cuvette and bubbling air in the cuvette (dark curves, "standard conditions") or by addition of buffer saturated with O_2 (light curves). [**Li**] = 12 µM, [Cu(II)] = 10 µM, [Asc] = 100 µM, [HEPES] = 100 mM, pH 7.4, T = 25 °C.

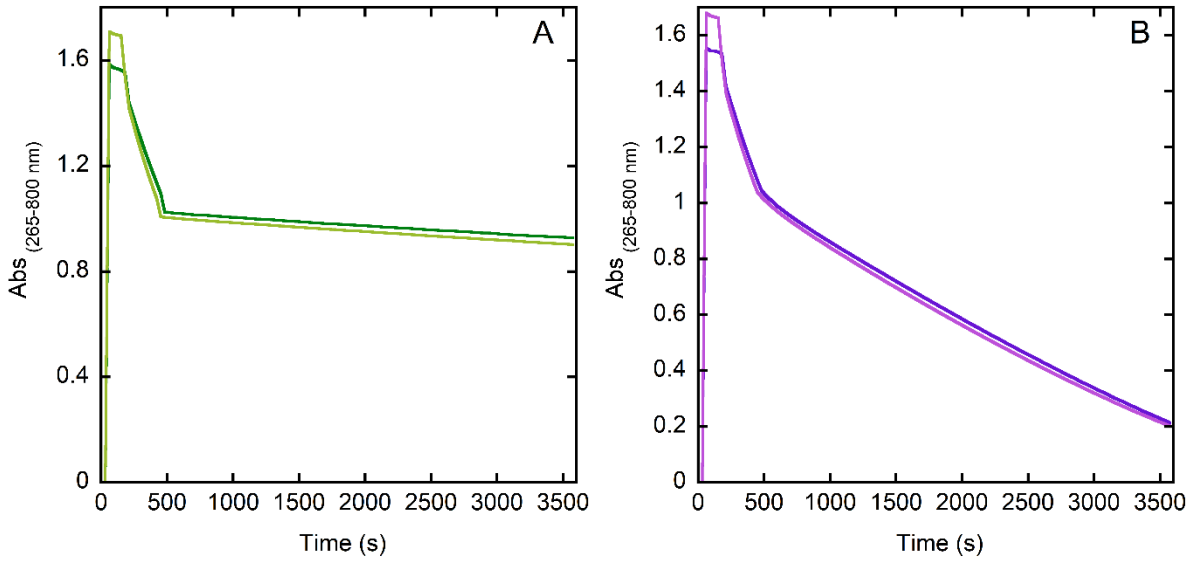

Figure S15. Kinetics of ascorbate consumption followed by UV-visible spectroscopy at 265 nm starting from Cu(I)/Cu(II) in the presence of (A) **L2**, (B) **L5** and $A\beta_{16}$ (dark curves) or $A\beta_{40}$ (light curves). [**Li**, Aβ] = 12 µM, [Cu(II)] = 10 µM, [Asc] = 100 µM, [HEPES] = 100 mM, pH 7.4, T = 25 °C.

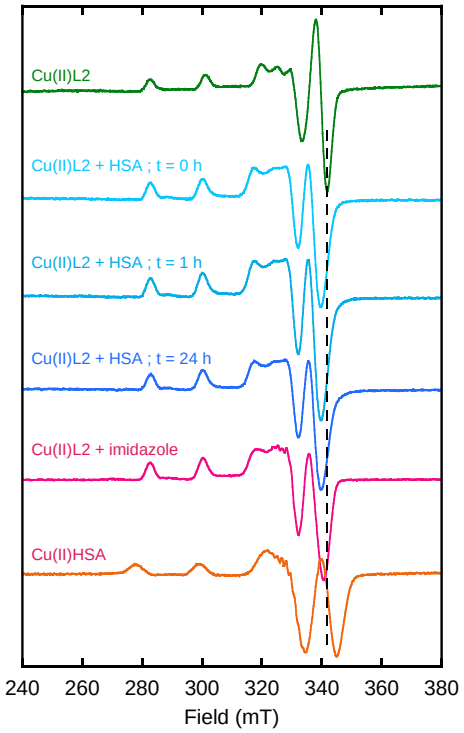

Figure 16. X-band EPR spectra of Cu(II)**L2** in the presence of one equiv. of HSA (Human Serum Albumin) at different time points. [**L2**] = [HSA] = 600 µM, [^{65}Cu(II)] = 500 µM, [HEPES] = 100 mM, pH 7.4, 10% of glycerol as cryoprotectant, 120 K.

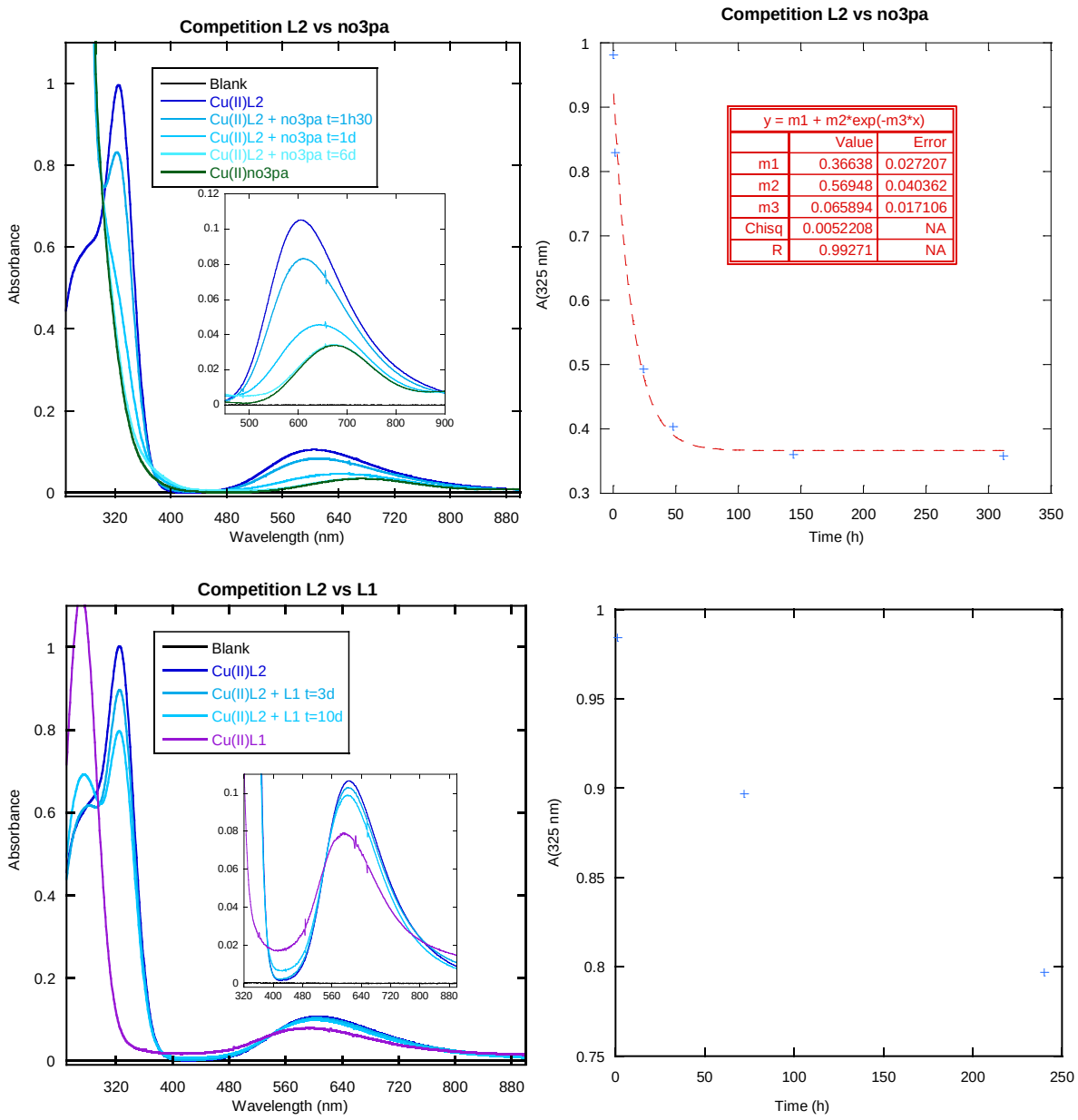

Figure S17. UV-Vis spectra and kinetics of ligand exchange of Cu(II)**L2** with addition of another ligand, ligand = no3pa or **L1**. Condition : [Cu(II)] = 240 µM, [ligand] = 290 µM, [HEPES] = 100 mM, pH 7.4, T= 25°C.

The removing of Cu(II) from Cu(II)**L2** by no3pa has been kinetically monitored at 325 nm. Using a mono-exponential decay, the $t_{1/2}$ is estimated to 10 hours. ($t_{1/2} = \frac{\ln(2)}{0.066} = 10h$).

The removing of Cu(II) from Cu(II)**L2** by **L1** has been kinetically monitored at 325 nm. The $t_{1/2}$ is much higher than 10 days.

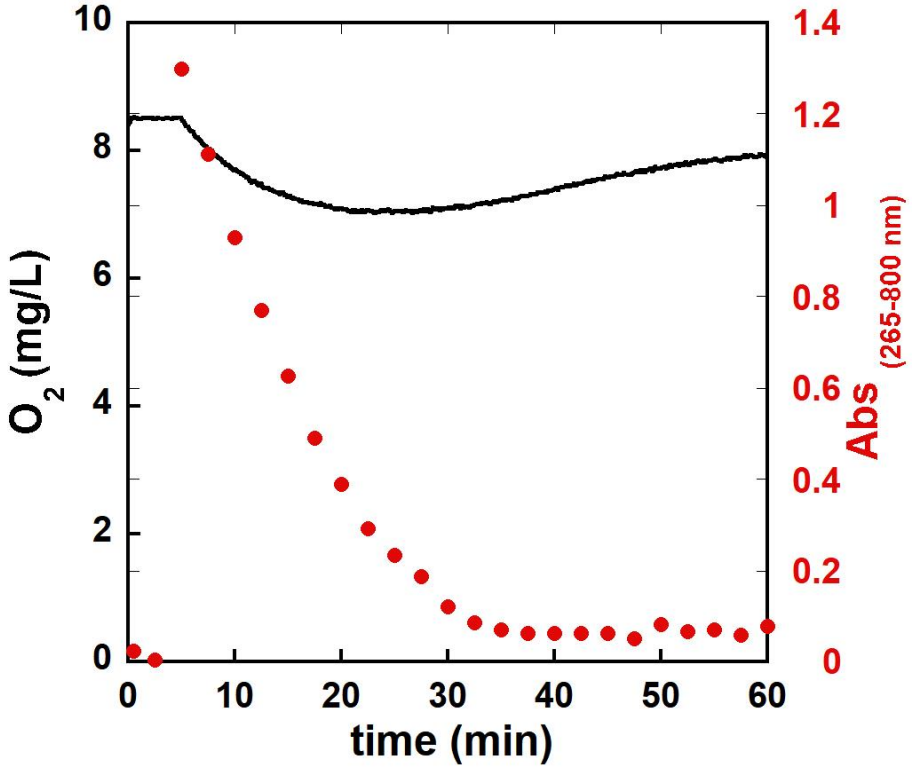

Figure S18. Dioxygen level measured by Clark electrode (black) and corresponding Asc concentration measured by UV-Vis (red dots). [O_2] = air satured conditions ; [Asc] = 100 µM, Cu = 10µM, Aβ = 12 µM in hepes buffer pH 7.4 100 mM. T = 22°C.

The measurements of O_2 level during Cu(Aβ)-induced ascorbate consumption was monitored with a similar set-up than the one of Ascorbate consumption since the Clark electrode was not suited to enter the UV-Vis cuvette. We have thus performed the reaction in a separate Becher in which we have measured the level of O_2 with the Clark electrode (Figure S18, black). Similar volume/air surface ratio and similar stirring was used to be as close as possible to the O_2 diffusion conditions encountered during the UV-Vis monitoring of ascorbate consumption. To secure that the kinetic of ascorbate consumption were similar in the Becher or UV-Vis cuvette, we also measured the level of ascorbate by taking 100µL aliquots of the solution and recording the corresponding UV-Vis spectrum (Figure S18, red dots).

References.

(1) Stoll, S.; Schweiger, A. *J. Magn. Reson.* **2006**, *178*, 42-55.
(2) Hancock, R. D.; Dobson, S. M.; Evers, A.; Wade, P. W.; Ngwenya, M. P.; Boeyens, J. C. A.; Wainwright, K. P. *J. Am. Chem. Soc.* **1988**, *110*, 2788-2794.
(3) Kodama, M.; Koike, T.; Hoshiga, N.; Machida, R.; Kimura, E. *J. Chem. Soc., Dalton Trans.* **1984**, 673-678.
(4) Balakrishnan, K. P.; Kaden, T. A.; Siegfried, L.; Zuberbühler, A. D. *Helv. Chim. Acta* **1984**, *67*, 1060-1069.
(5) Aragoni, M. C.; Arca, M.; Bencini, A.; Blake, A. J.; Caltagirone, C.; Decortes, A.; Demartin, F.; Devillanova, F. A.; Faggi, E.; Dolci, L. S.*et al. Dalton Transactions* **2005**, 2994-3004.
(6) Guillou, A.; Lima, L. M. P.; Roger, M.; Esteban-Gómez, D.; Delgado, R.; Platas-Iglesias, C.; Patinec, V.; Tripier, R. *Eur. J. Inorg. Chem.* **2017**, *2017*, 2435-2443.
(7) Kirsipuu, T.; Zadorožnaja, A.; Smirnova, J.; Friedemann, M.; Plitz, T.; Tõugu, V.; Palumaa, P. *Sci. Rep.* **2020**, *10*, 5686.
(8) Rozga, M.; Sokolowska, M.; Protas, A. M.; Bal, W. *J. Biol. Inorg. Chem.* **2007**, *12*, 913-918.
(9) Alies, B.; Renaglia, E.; Rozga, M.; Bal, W.; Faller, P.; Hureau, C. *Anal. Chem.* **2013**, *85*, 1501-1508.
(10) Noël, S.; Perez, F.; Ladeira, S.; Sayen, S.; Guillon, E.; Gras, E.; Hureau, C. *J. Inorg. Biochem.* **2012**, *117*, 322-325.